Ppb-Level Quartz-Enhanced Photoacoustic Detection of Carbon Monoxide Exploiting a Surface Grooved Tuning Fork

Ppb-level quartz-enhanced photoacoustic detection of carbon monoxide exploiting a surface grooved tuning fork

Shangzhi Li,[†,‡] Lei Dong,[*,†,‡] Hongpeng Wu,[†,‡] Angelo Sampaolo,[§] Pietro Patimisco,[§] Vincenzo Spagnolo[†,§] and Frank K. Tittel[⁄⁄]

[†] State Key Laboratory of Quantum Optics and Quantum Optics Devices, Institute of Laser Spectroscopy, Shanxi University, Taiyuan 030006, China

[‡] Collaborative Innovation Center of Extreme Optics, Shanxi University, Taiyuan 030006, China

[§] PolySense Lab – Dipartimento Interateneo di Fisica, University and Politecnico of Bari, Via Amendola 173, Bari, Italy

[⁄⁄] Department of Electrical and Computer Engineering, Rice University, Houston, Texas 77005, USA

ABSTRACT: A compact and sensitive carbon monoxide (CO) sensor was demonstrated by using quartz enhanced photoacoustic spectroscopy (QEPAS) exploiting a novel 15.2 kHz quartz tuning fork (QTF) with grooved surfaces. The custom QTF was designed to provide a quality factor as high as 15,000 at atmospheric pressure, which offers a high detection sensitivity. A large QTF prong spacing of 800 μm was selected, allowing to avoid the use of any spatial filters when employing a quantum cascade laser (QCL) as the excitation source. Four rectangular grooves were carved on the surfaces of two QTF prongs to decrease the electrical resistance and hence enhance the signal amplitude. With water vapor as the catalyst for vibrational energy transfer, the sensor system using the novel surface grooved QTF achieved a CO minimum detection limit (1σ) of 7 ppb for a 300-ms averaging time, which corresponds to a normalized noise equivalent absorption (NNEA) coefficient of 8.74×10^{-9} $cm^{-1}W/\sqrt{Hz}$. Continuous measurements covering a seven-day period for atmospheric CO were performed to demonstrate the stability and robustness of the developed CO sensor system.

Carbon monoxide (CO) is a colorless, odorless, poisonous gas, and represents one of the key contributors to the atmospheric pollution. The main sources of CO emission into the atmosphere come from the incomplete combustion of carbonaceous fuels, including automobile exhaust, heating boiler, power generation, coking and steel fabrication. Currently, CO is one of the pollutants with high concentration levels in the troposphere, which has a significant impact on both atmospheric chemistry and global climate through its reaction with hydroxyl (OH) for troposphere ozone formation.[1-5] Therefore, the concentration level of CO is an important indicator in daily urban air pollution index. The current method used by the US Environmental Protection Agency (EPA) for automated and continuous monitoring of ambient CO mixing ratio is the non-dispersive infrared (NDIR) technique, which has a detection limit of 50 ppbv with a response time of 5 min and a precision of 0.2 ppmv.[6] However, according to the report on carbon monoxide trends provided by US EPA, average CO concentrations in USA have decreased from 4.0 ppmv in 1997 to 1.2 ppmv in 2017. For a good air quality day, the CO mixing ratio can even be <150 ppb.[7] The availability of a compact CO sensor with ppb-level detection sensitivity and a fast response will allow real time monitoring and precise quantification of CO urban and industrial emission. Furthermore, this kind of CO sensors could be employed in smart traffic lights to regulate the traffic flow through cities and reduce pollution hot spots.

Quartz enhanced photoacoustic spectroscopy (QEPAS) since its first demonstration in 2002 has proved to be a robust and sensitive trace-gas optical detection technique, in which a quartz tuning fork (QTF) acoustically coupled with an acoustic micro-resonator (AmR) tube is employed as a resonant acoustic transducer to detect weak photoacoustic excitation.[8,9] The QTF and the AmR tube form a QEPAS spectrophone.[10] The AmR tube acts as an acoustic resonator for the QTF and then the length and the inner diameter of the tube have to be optimized to obtain the highest sound amplification, based on the QTF resonance frequency. Due to the small size of the QTF-based spectrophone, the QEPAS technique sets the basis for producing compact and robust gas sensors operating with extremely small gas volumes.[10-23] The fundamental vibration band of CO molecule with the strongest absorption coefficient is located at ~4.6 μm, which can be targeted by mid-infrared (MIR) quantum cascade lasers (QCLs). Many efforts were made so far to implement single mode QCL sources into QEPAS sensors while preserving compactness.[24] However, QEPAS based MIR sensor systems are difficult to be made compact. With respect to the near-infrared (NIR) laser diodes, the larger beam size in the wavelength range of >3 μm poses higher demands in terms of beam focusing, even if good beam-quality QCLs are employed as excitation source. When compact distributed-feedback (DFB) QCLs are employed, spatial filters should be implemented for beam shaping before directing the laser beam into the spectrophone, significantly increasing the footprint of the sensor system. Furthermore, in order to allow MIR laser beam easier to pass through, the length and the inner diameter of the used AmR tubes must be shortened and enlarged, respectively. This results in an overall degeneration of sensor performance.

The main QTF geometrical parameter influencing the optical coupling between the laser source and the QEPAS spectrophone is the gap between the two prongs, since a narrow spacing can easily block a portion of laser beam and produce an undesirable fringe-like background.[25,26] This occurs when a standard 32.7 kHz QTF with a prong spacing of 300 μm is used without employing a spatial or laser modal beam filter. A QTF with a larger prong spacing permits the use of the AmR tubes with larger inner diameters, thereby allowing a MIR laser beam to pass easily through the spectrophone without hitting it. Moreover, a proper design of the prong geometry can reduce the QTF resonance frequency.[27,28] This is helpful to enhance the CO signal amplitude, due to the fact that a mandatory condition for an effective sound wave generation is that the molecular relaxation time τ should be far shorter than the modulation period. Otherwise it can cause a reduction of the photoacoustic signal when using QEPAS to detect molecules with a slow Vibration-Translation (V-T) relaxation, such as CO.[24,27-31] Therefore, QTF customization by varying the prongs geometry and size, is very useful for QEPAS sensing applications depending on the specific laser source, target gas and sensing application. The biggest challenge in the design is to reduce the resonance frequency while keeping the high QTF quality factor and the low electrical resistance, since these QTF parameters significantly affect the QEPAS spectrophone performance, as demonstrated in several publications.[33-36]

In this manuscript, we report a ppb-level MIR CO sensor system based on QEPAS, in which a novel custom QTF with grooves applied on both surfaces is designed and employed. The grooved QTF has a resonance frequency of 15.2 kHz with a quality factor of 15,000 at atmospheric pressure in air and a prong spacing of 800 μm, which perfectly match a MIR laser beam. Grooves applied on both surfaces allowed a significant reduction of the QTF electrical resistance. These features permit the QEPAS sensor system to employ a DFB QCL as the excitation source with high detection sensitivity, but without the use of spatial or laser modal beam filters, thus making the sensor system robust and compact.

EXPERIMENTAL SECTION

Design methodology of QTFs for CO sensing. The grooved QTF is schematically shown in Figure 1. The prong length *l*, width *w*, thickness *t* and prong spacing *g* of the custom QTF are 9.4 mm, 2 mm, 0.25 mm and 0.8 mm, respectively, as shown in Figure 1A, which were determined based on the following design consideration. According to Euler-Bernoulli model,[27,34,35] the fundamental resonance frequency *f* of the QTF is related to its geometric parameters, which is given by:

$$f = \frac{1.194^2\,\pi\, w}{8\sqrt{12}\,l^2}\sqrt{\frac{E}{\rho}} \propto \frac{w}{l^2} \qquad (1)$$

where E is the elastic Young modulus of the quartz (0.72×10^{11} N/m^2) and ρ is the density of the quartz (2,650 kg/m^3).

The electrical resistance *R* of the QTF represents the loss in the equivalent resonator circuit, determining the charge generation capability. Theoretically, *R* is related to geometrical parameters by the following relation: [37]

$$R \propto \frac{l^2}{t\sqrt{w}} \qquad (2)$$

The *Q*-factor is determined by all the energy dissipation mechanisms occurring in a vibrating QTF prong, such as losses due to the surrounding fluid, support loss, surface, volume and thermo-elastic losses. All these losses strongly depend on the dimensions of the QTF prongs. Each loss contribution is independent from the others, but all occur simultaneously. No theoretical model can take into account all the dissipation mechanisms using a single and concise formulation. But an empirical equation related to the prong size was provided according to a large number of experimental datasets as:[36]

$$Q = 3.78 \times 10^5 \frac{wt}{l} \qquad (3)$$

As discussed in the previous section, a QTF designed to easily accommodate MIR laser beams and operate properly with slow relaxing gases should have the following characteristics: 1) large prong gap to facilitate the optical alignment and reduce the optical background noise; 2) resonance frequency low enough to adapt to the relaxation rate of target gas; 3) a high *Q*-factor to achieve a high signal amplitude and detection sensitivity; 4) low electrical resistance to enhance charge generation capability. The resonance frequency, the *Q*-factor and the electrical resistance are figures of merit strongly interrelated with each other. In fact, to reduce *f*, one has to design QTFs with small width *w* and large prong length *l* (see Eq. (1)), which produce large electrical resistance (Eq. (2)) and a low *Q*-factor (Eq. (3)). In principle, a larger thickness *t* can be adopted in order to compensate the *Q*-factor loss. However, chemical etching of a crystal of $t > 1$ mm cannot guarantee sharp edge profiles. Conversely, short *l* and large *w* offers a good quality factor and electrical resistance, but resulting in an increase of the resonance frequency.

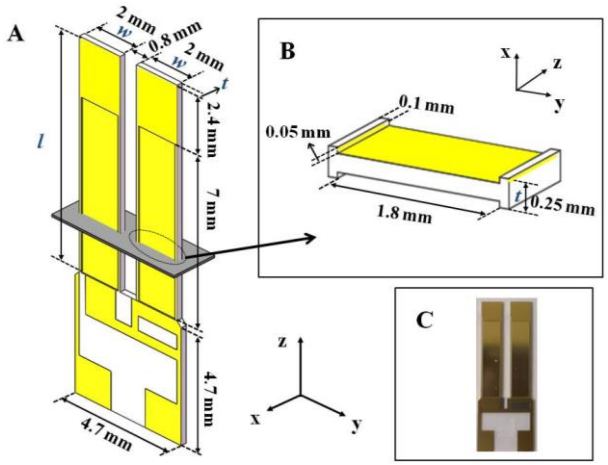

Figure 1. (A) Schematic of the geometrical dimensions of the grooved tuning fork. The yellow areas represents the section of electrode layout. (B) Cross-section of grooves on the QTF. (C) Photograph of the novel grooved QTF.

Considering that the V-T relaxation of CO molecule is in the order of ~10 μs,[38] a resonance frequency of 16 kHz was selected. The thickness *t* is fixed to 0.25 mm. A larger prong width *w* is helpful to improve the *Q*-factor. However the ratio of *t*/*w* must be >0.1 in order to ensure the match between the prong mass and the sound pressure exerted on the lateral surface of the prong. Therefore, a 2-mm width *w* was used. The prong length can be subsequently determined by Eq. (1) to be 9.4 mm. With these prong size, a theoretical *Q* factor of ~20,000 was estimated by using Eq. (3).

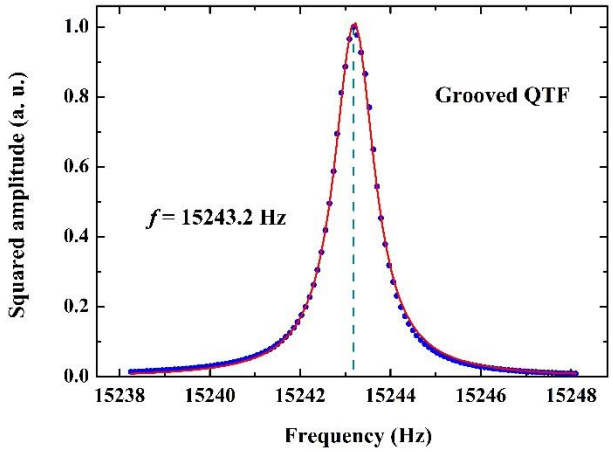

Figure 2. Frequency response curve of the grooved QTF at atmospheric pressure in air. The red line indicates a Lorentzian fit.

In order to decrease the electrical resistance, four rectangular grooves, each one having dimensions of 1.8 × 7 × 0.05 mm^3, were carved on both surfaces of the two QTF prongs, as shown in Figure 1. Approximately 40% of the QTF thickness was removed and the central electrodes were deposited on the carved surfaces. The presence of the grooves reduces the distance between the different electrodes of QTF and thus increasing the piezoelectric coupling. As a result, a reduction of the electrical resistance is expected. The prong surface grooving does not affect the *Q*-factor of the QTF.

Table 1. Electrical parameters (resonance frequencies *f*, *Q*-factor and electrical resistance *R*) measured for QTF#1 and QTF#2. The theoretical values for the resonance frequency *f* and *Q*-factor are also reported.

	f (Hz)	*Q*	*R* (kΩ)
Theoretical value	16,000.0	20,100	-
QTF#1	15,846.9	15,408	153.97
QTF#2	15,243.2	15,022	107.15

The grooved QTFs were fabricated stating from a Z-cut quartz crystal plate and a cutting angle of 2 degrees with respect to the crystallographic X-axis, by using standard photolithographic techniques and chemical etching.[39] Subsequent the four grooves were carved. For comparison purpose, a QTF with same geometric parameters, but without carved grooves was also fabricated. Gold patterns were deposited to collect the electrical charge. The resonance properties of the grooved QTFs were measured using electrical excitation method (Figure S1). The response curve of a grooved QTF was shown in Figure 2. The response (squared amplitude) fits well to a Lorentzian line shape. The theoretical and experimental electrical parameters from two QTFs without and with the carved grooves, marked by QTF#1 and QTF#2, respectively, are listed in Table 1. The experimental results of QTF#1 is in good agreement with the theoretical estimation. As expected, the addition of the grooves does not affect the *Q*-factor, while the resonance frequency decreases of < 4%. At the same time, the electrical resistance is reduced by ~ 30% (~ 50 kΩ).

CO sensor design based on a grooved QTF. A schematic of the experimental setup used to demonstrate the performance of the QEPAS-based CO sensor employing a grooved QTF is shown in Figure 3. The QEPAS spectrophone consisted of a grooved QTF and AmRs in dual-tube on-beam configuration, *i.e.* a stainless-steel tube is cut into two pieces and the grooved QTF is inserted between them. The spectrophone was placed in a gas cell with outside dimensions of ~130 cm^3. Two CaF_2 windows with diameters of 25.4 mm and transmissivity efficiency of >95% were mounted on the gas cell to allow the laser beam to pass through. The gas cell including the spectrophone is called an acoustic detection module (ADM). A DFB-QCL (AdTeck optics, Model HHL-17-62) with a central wavelength of 4.61μm was employed as the excitation source to generate the photoacoustic signals. The QCL was packaged with internal optics providing a collimated laser beam with a diameter of 2.7 mm at 1.1 m and a divergence angle of 1 mrad. The temperature of the DFB-QCL was set to 38.5 °C by means of a temperature controller (Thorlabs, Model TED200C), while its current was controlled by a current driver (Wavelength Electronics, Model QCL2000LAB). A 75-mm focal length plano-convex CaF_2 lens was used to focus the collimated laser beam into a ~0.20 mm^2 circular spot at the focal point with a Rayleigh length of 4.3 cm, so that the laser beam can easily pass through the dual tube spectrophone located inside the ADM. A power meter (Ophir Optronics Solutions. LTD, Israel, Model 3AROHS) was placed behind the ADM to monitor the optical power for alignment purpose.

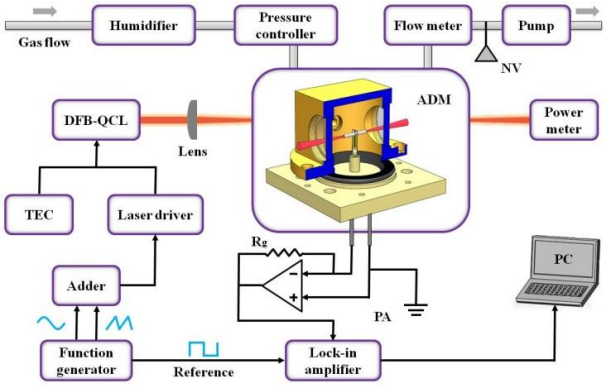

Figure 3. Schematic diagram of QEPAS-based CO sensor system using a novel grooved QTF. TEC: temperature controller; NV: needle valve and TA: pre-amplifier.

To carry out a sensitive quantitative CO concentration measurement, the 2*f* wavelength modulation photoacoustic detection approach was employed.[22,25,40] A wavelength modulation of the QCL was obtained by applying a sinusoidal dither to the current of the DFB-QCL at half of the grooved QTF resonance frequency ($f = f_0/2$ ~7.6 kHz). A low ramp wave from a function generator was added to sinusoidal dither by means of an electrical adder to enable the laser wavelength scanning across the selected CO absorption line. The piezoelectric current generated by the grooved QTF was converted into an output voltage by a trans-impedance preamplifier with a 10 MΩ feedback resistor. Then this voltage signal was demodulated at f_0 by using a lock-in amplifier (Stanford Research Systems, Model SR830). The filter slope and the time constant of the lock-in amplifier

were set to a 12 dB/oct filter slope and 300 ms time constant, corresponding to a detection bandwidth of Δf =0.833 Hz.

A silicone hollow fiber membrane module (PermSelect@, Model PDMSXA-2500), providing an addition of ~ 2.5 % water vapor concentration, was employed as a humidifier to efficiently improve the CO vibrational-translational (V-T) relaxation processes within the gas mixture. The gas pressure in the ADM was controlled at 700 Torr by a compact pressure controller (MKS Instrument Inc., USA, Model 649B) and a mini diaphragm pump (KNF Technology Co., LTD, Germany, Model N813.5ANE). The flow rate of gas through the ADM was set to a constant value of 80 sccm via a needle valve. A mass flow meter (Alicat Scientific, Inc. Model M-500SCCM-D) was used to monitor the gas flow rate.

RESULTS AND DISCUSSION

Performance assessment of sensor system. The geometrical parameters of the AmR used in the spectrophone were first optimized in order to obtain the best performance of the CO sensor system based on the grooved QTF (Figure S2). The results show that two metallic tubes with a length of 9.00 mm and an inner diameter of 1.65 mm yielded a maximum signal-to-noise ratio (SNR) gain factor of 28 when each tube was mounted 20 μm away from the QTF surface and 1.5 mm below the QTF top. According to the HITRAN database and Ref. [7], the R(6) CO absorption line located at 2,169.2 cm^{-1} with a line-strength of 4.5×10^{-19} cm/mol was selected for the sensor operation since it is interference-free from other gases in ambient air. The temperature and central current of the DFB-QCL were set to 38.5 ºC and 212 mA, respectively, in order for the DFB-QCL to target the selected R(6) line. A ramp wave from 202 mA to 222 mA allows retrieving a complete 2*f* profile of the R(6) line. A certificated mixture of 1 ppm CO in N_2 (Beijing AP BAIF Gases Industry CO, Ltd) with an uncertainty of 2% was used to determine the best operating conditions for the CO sensor based on the grooved QTF. A 2.5% water vapor concentration was added into the gas mixture flowing through the ADM. To maximize the amplitude of the QEPAS signal, the modulation depth was chosen appropriately (Figure S3). With an optimized modulation depth of 15 mA, the signal amplitude of the CO 2*f* spectrum reached to 243 μV, as shown in Figure 4. The noise level of the CO QEPAS sensor was measured and determined to be 1.62 μV when the humidified N_2 was introduced. With a data acquisition time of 1 sec, the 1σ minimum detection limit of 7 ppb was obtained for the QCL optical power of 21 mW, which is ~ one order of magnitude higher than the NDIR technique[4]. Such a detection limit corresponds to a normalized noise equivalent absorption (NNEA) coefficient of 8.7×10^{-9} $cm^{-1}W/\sqrt{Hz}$, 1.9 and 1.7 times better than the two reported for standard QTF based CO QEPAS sensors using a DFB-QCL with a spatial filter (1.61×10^{-8} $cm^{-1}W/\sqrt{Hz}$) or an EC-QCL (1.48×10^{-8} $cm^{-1}W/\sqrt{Hz}$), respectively.[7,24]

In order to verify that the addition of water vapor can efficiently improve the CO V-T relaxation processes and hence enhance the CO signal amplitude, the humidifier was removed from the gas line and the dry 1-ppm CO/N_2 gas mixtures was introduced to the ADM. The obtained spectrum is also shown in Figure 4. As a result, a gain factor of ~8 on the peak value of the QEPAS spectra is measured when 2.5% of water vapor is added to the CO/N_2 mixture.

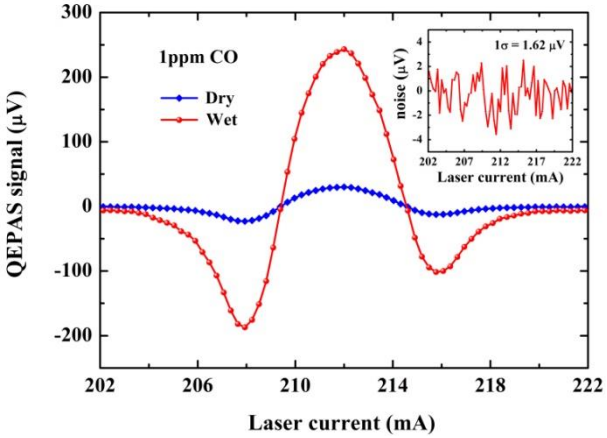

Figure 4. Experimental measured 2*f*-QEPAS spectra for dry and wet CO/N_2 gas mixtures, both containing 1 ppmv CO concentration at atmospheric pressure. The inset shows the 1σ noise level with wet pure N_2.

For online and real time measurements, the sensor response time is an important parameter to be estimated. A fast response time can reduce the data delay and provide a quasi-real time monitoring. The gas cell has an inner volume of 70 cm^3 due to the small size of the grooved QTF-based spectrophone. Such a small volume provides a fast gas exchange rate, so that quick concentration variations can be captured. As an optical sensing technique, the response time of QEPAS sensors is completely determined by the gas exchange rate. With a fixed volume, a faster gas flow can achieve a faster response time. However, a large gas flow may create unwanted QTF prong vibration causing an increase of the ADM noise level. The relationship between the gas flow and the ADM noise was investigated (Figure S4). An increase of noise was not observed for flow levels up to 80 sccm. Therefore, 80 sccm was selected for the sensor operation, corresponding to a theoretical gas exchange time of 53 s.

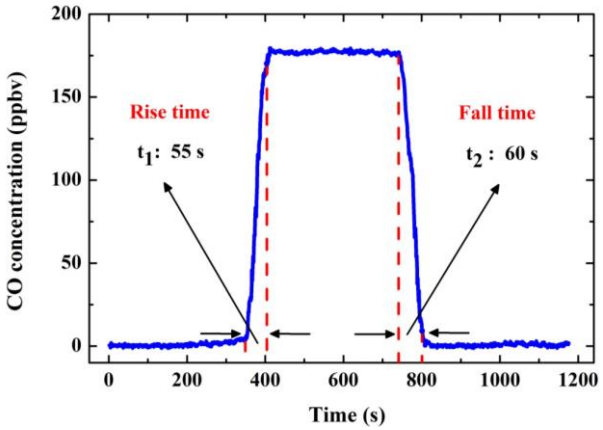

Figure 5. Rise time and fall time of the sensor system based on a grooved QTF. Rise time: the time interval between initial response and 95% of the final response. Fall time: the time interval between initial response to a step decrease in concentration and 95% of the final response.

To verify the theoretical prediction, the actual response time was measured by using the following three-step procedure, as

shown in Figure 5. First, pure nitrogen was fed into the sensor system and then the gas source was rapidly switched to the 180 ppbv CO/N_2 mixture produced by the dilution system to measure the signal rise time. Finally, pure nitrogen was again introduced into sensor system to measure the fall time. The QEPAS signal was recorded while the wavelength of the laser source was locked at the CO absorption line peak. The same definitions of rise and fall time as in the US EPA report was used.[6] The obtained rise and fall times are 55 s and 60 s, respectively, which are in excellent agreement with the theoretical prediction of 53 s, considering the volume of the gas line. The obtained response time is ~ 5 times less than that reported for NDIR technique.[6]

Continuous monitoring of atmospheric CO mixing ratios. The wavelength of the sensor system based on a grooved QTF was locked at the absorption line center, so that the amplitude of the 2*f* signal was directly measured as a function of the time. The field application of the CO sensor with a 1-s acquisition time was demonstrated by continuous monitoring of atmospheric CO. The sensor system was placed in the Shaw Amenities Building on the Shanxi University campus in Taiyuan, China. A gas sampling system was appropriately realized to acquire air from outdoors by use of a Teflon tube. A 3 μm and 1.2 μm micro-pore hydrophobic PTFE filter membranes were mounted at air inlet as 1st stage air filter in order to avoid the contamination by dust or soot particles, and in front of the ADM as 2nd stage air filter in order to filter the water droplets, respectively. The humidifier provided a 2.5 % water vapor concentration into the sampled gas flow. The CO concentrations measured for seven days of continuous monitoring (Nov. 21, 2018 to Nov. 27, 2018) are shown in Figure 6A. For comparison, the CO concentration data released by the China National Environmental Monitoring Center (CNEMC)[41] are shown in Figure 6B. This data was acquired by an environmental monitoring station, which is located 7 km from our sensor system and uses a NDIR method with a lower detectable limit of 50 ppbv (Satellite map shown as Figure S5). The variation trend of atmospheric CO concentration measured by the grooved QTF based CO sensor system is in excellent agreement with Figure 6B. The NDIR system suffers from a very slow data updating rate (1 data point/hours) while the ability of high sensitivity and fast response of the CO sensor based on a grooved-QTF allows for a much higher sampling and detection rate, and therefore it is possible to measure the CO concentration evolution in time with a higher precision. For example, several oscillations at high concentration levels were recorded at ~8:00 a.m. (0:00 a.m. GMT), on Nov. 27, 201 8 in Figure 6A. A similar behavior was not observed in Figure 6B since all data within 1 hour was averaged. At some specific moments, such as 8:00 a.m. (0:00 a.m. GMT) on Nov. 24, 10:00 a.m. (2:00 a.m. GMT) on Nov. 25 and 9:00 a.m. (1:00 a.m. GMT) on Nov. 26, the concentration values published by the CNEMC are higher than those obtained by the grooved QTF based sensor. On the contrary, the concentration values published by CNEMC were lower at 9:00 p.m. (1:00 p.m. GMT) on Nov. 25 and on Nov. 27. These small differences are mostly due to the distance between two sensor systems (7 kilometers) and local CO concentration variations.

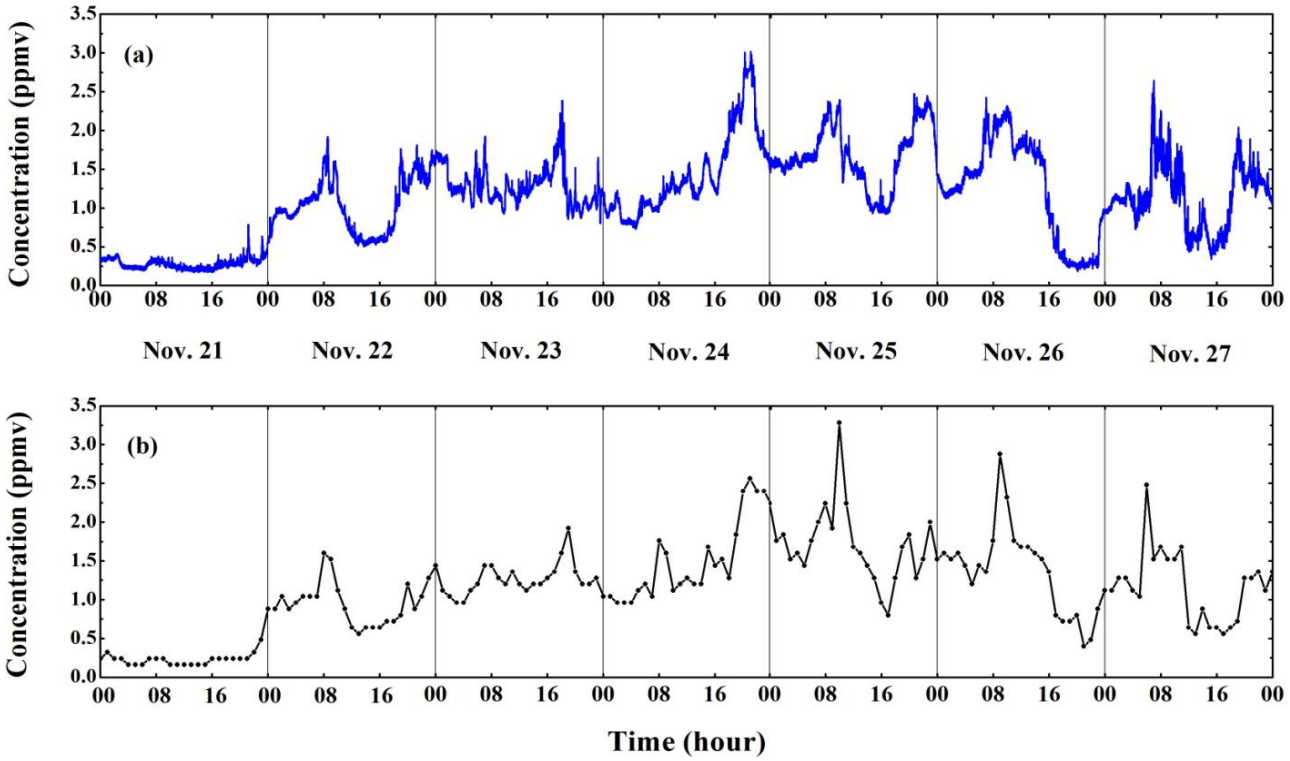

Figure 6. (A) Continuous monitoring of atmospheric CO concentrations measured during a seven-day period in Nov. 2018 on the Shanxi University, Taiyuan, China. (B) Corresponding data available from a nearby station of the Department of Ecology and Environment of Shanxi Province.

CONCLUSIONS

A novel grooved QTF was designed with an 800-μm prong spacing and 15.2-kHz resonance frequency with a quality factor as high as 15,000 at atmospheric pressure in air. The modification of four rectangular grooves on the prong surface reduces the electrical resistance and thus further enhances the signal amplitude. It was demonstrated that the novel grooved QTF can be used for ppb-level CO detection with a commercially available small-size DFB-QCL. The detection limit of the sensor system based on the grooved QTF is ~ 1 order of magnitude better than commercial NDIR sensor and ~ 2 times better than the best detection limit obtained with the QEPAS sensor system based on a standard 32.7 kHz QTF. Moreover, the additional advantages of a fast response time and a small size were achieved. The QEPAS sensor was tested for out-of-laboratory applications by a continuously monitoring of atmospheric CO for seven days. The data obtained are in excellent agreement with that recorded by the CNEMC monitoring station, thus validating the performance of the grooved QTF-based QEPAS sensor system. These features represent a solid starting point for developing a bench top prototype into a portable device for on field applications. Finally, since QEPAS response is directly proportional to the laser power, the concentration detection limits can be further improved if higher power QCL sources become available.

ASSOCIATED CONTENT

Supporting Information

The Supporting Information is available free of charge on the ACS Publications website.

Circuit diagram for QTF electrical excitation; QEPAS peak signal as a function of the inner diameter (panel A) and the length (panel B) of the acoustic resonator tubes; CO QEPAS signal amplitude measured as a function of the current modulation depths for a 1 ppm CO:N_2 gas mixture; Dependence of QEPAS noise level measured for pure N_2 as a function of the gas flow rate in the range of 20-140 sccm; Satellite map of the environmental station and the location where the QEPAS sensor system was placed.

AUTHOR INFORMATION

Corresponding Author

* E- mail: donglei@sxu.edu.cn.

ORCID

Lei Dong: 0000-0001-7379-3388

Author Contributions

All authors have given approval to the final version of the manuscript.

Notes

The authors declare no competing financial interest.

ACKNOWLEDGMENT

National Key R&D Program of China (2017YFA0304203), National Natural Science Foundation of China (NSFC) (61622503, 61575113, 61805132, 11434007), Changjiang Scholars and Innovative Research Team in University of Ministry of Education of China (IRT_17R70), 111 project (D18001), Outstanding Innovative Teams of Higher Learning Institutions of Shanxi, Foundation for Selected Young Scientists Studying Abroad, Sanjin Scholar (2017QNSJXZ-04) and Shanxi "1331KSC". Frank K. Tittel acknowledges support by the Robert Welch Foundation (Grant #C0586) The authors from Dipartimento Interateneo di Fisica di Bari acknowledge the financial support from THORLABS GmbH, within the joint-research laboratory PolySense.

REFERENCES

(1) Khalil, M.; Rasmussen, R. Science **1984**, *224*, 54-56.
(2) Logan, J. A.; Prather, M. J.; Wofsy, S. C.; McElroy, M. B. J. Geophys. Res. **1981**, *86*, 7210-7254.
(3) Ravishankara, A. R.; Daniel, J. S.; Portmann, R. W. Science **2009**, *326*, 123-125.
(4) Zhao, W.; Dong, M.; Chen,W.; Gu, X.; Hu, C.; Gao, X.; Huang, W.; Zhang, W. Anal. Chem. **2013**, *85*, 2260-2268.
(5) Zhao, W.; Fang, B.; Lin, X.; Gai, Y.; Zhang, W.; Chen, W.; Chen, Z.; Zhang, H.; Chen, W. Anal. Chem. **2018**, *90*, 3958-3964.
(6) United states environmental protection agency; *Air Quality Criteria for Carbon Monoxide*. Washington, 2000, EPA 600/P-99/001F.
(7) Ma, Y.; Lewicki, R.; Razeghi, M.; Tittel, F. K. Opt. Express **2013**, *21*, 1008-1019.
(8) Kosterev, A. A.; Tittel, F. K.; Serebryakov, D. V.; Malinovsky, A. L.; Morozov, I. V. Rev. Sci. Instrum. **2005**, *76*, 043105.
(9) Kosterev, A. A.; Bakhirkin, Y. A.; Curl, R. F.; Tittel, F. K. Opt. Lett. **2002**, *27*, 1902-1904.
(10) Dong, L.; Kosterev, A. A.; Thomazy, D.; Tittel, F. K. Appl. Phys. B **2010**, *100*, 627-635.
(11) Patimisco, P.; Scamarcio, G.; Tittel, F. K.; Spagnolo, V. Sensors **2014**, *14*, 6165-6206.
(12) Patimisco, P.; Sampaolo, A.; Dong, L.; Tittel, F. K.; Spagnolo, V. Appl. Phys. Rev. **2018**, *5*, 011106.
(13) Dong, L.; Wu, H.; Zheng, H.; Liu, Y.; Liu, X.; Jiang, W.; Zhang, L.; Ma, W.; Ren, W.; Yin, W.; Jia, S.; Tittel, F. K. Opt. Lett. **2014**, *39*, 2479-2482.
(14) Mordmüller, M.; Köhring, M.; Schade, W.; Willer, U. Appl. phys. B **2015**, *119*, 111-118.
(15) Liu, K.; Guo, X.; Yi, H.; Chen, W.; Zhang, W.; Gao, X. Opt. Lett. **2009**, *34*, 1594-1596.
(16) Ren, W.; Jiang, W.; Sanchez, N. P.; Patimisco, P.; Spagnolo, V.; Zah, C.; Xie, F.; Hughes, L. C.; Griffin, R. J.; Tittel, F. K.; Appl. Phys. Lett. **2014**, *104*, 041117.
(17) Waclawek, J. P.; Moser, H.; Lendl, B. Opt. Express **2016**, *24*, 6559-6571.
(18) Wu, H.; Dong, L.; Zheng, H.; Liu, X.; Yin, X.; Ma, W.; Zhang, L.; Yin, W.; Jia, S.; Tittel, F. K. Sens. Actuators, B **2015**, *221*, 666-672.
(19) Tittel, F. K.; Allred, J. J.; Cao, Y.; Sanchez, N. P.; Ren, W.; Jiang, W.; Jiang, D.; Griffin, R. J. Int. Soc. Opt. Photonics. **2015**, *9370*, 93700V.
(20) Wang, Z.; Li, Z.; Ren, W. Opt. Express **2016**, *24*, 4143-4154.
(21) Zheng, H.; Dong, L.; Yin, X.; Wu, H.; Zhang, L.; Ma, W.; Yin, W.; Jia, S. Sens. Actuators, B **2015**, *208*, 173-179.
(22) Wu, H.; Dong, L.; Zheng, H.; Yu, Y.; Ma, W.; Zhang, L.; Yin, W.; Xiao, L.; Jia, S.; Tittel, F. K. Nat. Commun. **2017**, *8*, 15331.
(23) Wu, H.; Dong, L.; Ren, W.; Yin, W.; Ma, W.; Zhang, L.; Jia, S.; Tittel, F. K. Sens. Actuators, B **2014**, *206*, 364-370.
(24) Dong, L.; Lewicki, R.; Liu, K.; Buerki, P. R.; Weida, M. J.; Tittel, F. K. Appl. Phys. B **2012**, *107*, 275-283.
(25) Dong, L.; Spagnolo, V.; Lewicki, R.; Tittel, F. K. Opt. Express **2011**, *19*, 24037-24045.
(26) Spagnolo, V.; Patimisco, P.; Borri, S.; Scamarcio, G.; Bernacki, B. E.; Kriesel, J. Appl. Phys. B **2013**, *112*, 25-33.
(27) Patimisco, P.; Sampaolo, A.; Dong, L.; Giglio, M.; Scamarcio, G.; Tittel, F. K.; Spagnolo, V. Sens. Actuators, B **2016**, *227*, 539-546.
(28) Patimisco, P.; Sampaolo, A.; Zheng, H.; Dong, L.; Tittel, F. K.;

Spagnolo, V. Adv. Phys. X **2017**, *2*, 169-187.
(29) Wu, H.; Sampaolo, A.; Dong, L.; Patimisco, P.; Liu, X.; Zheng, H.; Yin, X.; Ma, W.; Zhang, L.; Yin, W.; Spagnolo, V.; Jia, S.; Tittel, F. K. Appl. Phys. Lett. **2015**, *107*, 111104.
(30) Sampaolo, A.; Patimisco, P.; Dong, L.; Geras, A.; Scamarcio, G.; Starecki, T.; Tittel, F. K.; Spagnolo, V. Appl. Phys. Lett. **2015**,*107*, 231102.
(31) Yin, X.; Dong, L.; Zheng, H.; Liu, X.; Wu, H.; Yang, Y.; Ma, W.; Zhang, L.; Yin, W.; Xiao, L.; Jia, S. Sensors **2016**, *16*, 162.
(32) Wu, H.; Yin, X.; Dong, L.; Pei, K.; Sampaolo, A.; Patimisco, P.; Zheng, H.; Ma, W.; Zhang, L.; Yin, W.; Xiao, L.; Spagnolo, V.; Jia, S.; Tittel, F. K. Appl. Phys. Lett. **2017**, *110*, 121104.
(33) Patimisco, P.; Sampaolo, A.; Giglio, M.; Mackowiak, V.; Rossmadl, H.; Gross, B.; Cable, A.; Tittel, F. K.; Spagnolo, V. Opt. Lett. **2018**, *43*, 1854-1857.
(34) Patimisco, P.; Borri, S.; Sampaolo, A.; Beere, H. E.; Ritchie, D. A.; Vitiello, M. S.; Scamarcio, G.; Spagnolo, V. Analyst **2014**, *139*, 2079-2087.
(35) Sampaolo, A.; Patimisco, P.; Pennetta, R.; Scamarcio, G.; Tittel, F. K.; Spagnolo, V. Int. Soc. Opt. Photonics. **2015**, *9370*, 93700X.
(36) Patimisco, P.; Sampaolo, A.; Mackowiak, V.; Rossmadl, H.; Cable, A.; Tittel, F. K.; Spagnolo, V. IEEE T. Ultrason. Ferr. **2018**, *65*, 1951-1957.
(37) Hirata, M.; Kokubun, K.; Ono, M.; Nakayama, K. J. Vac. Sci. Technol. A **1985**, *3*, 1742-1745.
(38) Cottrell, T. L.; McCoubrey, J. C. *Molecular Energy Transfer in Gases*; Butterworths: London, 1961.
(39) Lee, S.; Lee, J. -Y.; Park, T. -S. Mater. Corros. **2001**, *52*, 712-715.
(40) Patimisco, P.; Sampaolo, A.; Bidaux, Y.; Bismuto, A.; Schott, M.; Jiang, J.; Muller, A.; Faist, J.; Tittel, F. K.; Spagnolo, V. Opt. Express 2016, 24, 25943-25954.
(41) China National Environmental Monitoring Center. http://www.cnemc.cn/.

for TOC only